scientific data

Check for updates

OPEN

DATA DESCRIPTOR

An open-access lumbosacral spine MRI dataset with enhanced spinal nerve root structure resolution

Jionghui Liu[1,4], Wenqi Zhang[1,4], Yuxing Zhou[1], Linhao Xu[1], Ying-Hua Chu[2] & Fumin Jia[1,3] ✉

Spinal cord injury (SCI) profoundly affects an individual's ability to move. Fortunately, recent advancements in neuromodulation, particularly the spatio-temporal epidural electrical stimulation (EES) targeting the spinal nerve roots, promoted rapid rehabilitation of SCI patients. Such neuromodulation techniques require precise anatomical modelling of spinal cord. However, the lack of spine imaging datasets, especially high-quality magnetic resonance imaging (MRI) datasets highlighting nerve roots, hinders the translation of EES into medical practice. To address this problem, we introduce an open-access lumbosacral spine MRI dataset acquired in 14 healthy adults, using constructive interference in steady state (CISS) sequence, double echo steady state (DESS) sequence, and T2-weight turbo spin echo (T2-TSE) sequence, with enhanced nerve root resolution. The dataset also includes the corresponding anatomical annotations of nerve roots and the final reconstructed 3D spinal cord models. The quality of our dataset is assessed using image quality metrics implemented in MRI quality control tool (MRIQC). Our dataset provides a valuable platform to promote a wide range of spinal cord neuromodulation research and collaboration among neurorehabilitation engineers.

Background & Summary

Spinal cord injury (SCI) is a profound trauma that significantly impacts the capability of affected individuals to generate functional standing and locomotor movements. Despite the limited availability of effective rehabilitation therapies for SCI in the past decades, recent advancements indicate the prospects of neuromodulation to enable individuals with SCI to stand and walk again. Specifically, the neural ensembles essential for generating standing and stepping are often situated below the injury site[1]. Therefore, activating the intact part of spine below the injury site via external stimulation could activate muscles in lower limb. Epidural electrical stimulation (EES), a neuromodulation technique empirically validated effective for pain relief[2], has emerged as a promising therapeutic approach for SCI rehabilitation. By targeting the posterior (sensory) nerve roots, EES exploits the intrinsic capacity of the spinal cord to use sensory signals as a source for movement control[3].

Traditional EES employs constant stimulation parameters[4,5]. However, constant EES alone has been proven insufficient for locomotor rehabilitation. The generation of natural, dynamic, and smooth lower-limb locomotion requires precise tuning of time-varying stimulation parameters, activating different nerve roots in different phases of movements. To this end, a novel approach, termed spatio-temporal EES[6], has emerged. Spatio-temporal EES precisely targets and switches between individual dorsal roots with predefined timing (in open-loop mode) or according to the feedback of current body postures (in closed-loop mode), replicating natural spatio-temporal activation patterns of spinal cord in a dynamic movement. By modulating specific motor neuron pools, spatio-temporal EES demonstrates superior rehabilitation performance[7,8]. Rowald *et al.*[6] applied spatio-temporal EES to three complete SCI patients, empowering them to stand, walk, cycle, swim, and manage trunk movements within a single day. Angeli *et al.*[9] reported successful overground walking recovery in two of four patients with motor complete paralysis after customized EES stimulation and intense physical training. Recent research[10] also integrated brain-spine interface (BSI) with spatio-temporal EES, enabling natural control of the lower-limb movements.

[1]Institute of Science and Technology for Brain-Inspired Intelligence, Fudan University, Shanghai, China. [2]MR Research Collaboration Team, Siemens Healthineers Ltd., Shanghai, China. [3]State Key Laboratory of Medical Neurobiology and MOE Frontiers Center for Brain Science, Fudan University, Shanghai, China. [4]These authors contributed equally: Jionghui Liu, Wenqi Zhang. ✉e-mail: jfmin@fudan.edu.cn

Spatio-temporal EES relies heavily on the precise identification and location of individual spinal nerve roots. Additionally, the medical translation of spatio-temporal EES is also constrained by the inter-individual variability of the human spinal cord[11]. To date, datasets specific to this area are scarce. Existing X-ray[12] or computed tomography (CT)[13,14] datasets primarily focus on vertebrae segmentation, neglecting distinct spinal nerve roots. Although magnetic resonance imaging (MRI) can provide clear nerve imaging, available spine MRI datasets predominantly support studies on chronic back pain[15,16] and cervical spondylosis[17], emphasizing the cervical[18] and spinal cord regions rather than spinal nerve roots. The lack of MRI datasets with enhanced spinal nerve root structure resolution remains a notable gap in the context of EES research.

To bridge this gap, we present an open-access lumbosacral spine MRI dataset with enhanced resolution of spinal nerve root structures. In this manuscript, we provide a detailed descriptions on our dataset, covering its design, acquisition, and preparation. Data quality is assessed using quality metrics implemented in MRI quality control tool (MRIQC)[19]. Furthermore, we provide anatomical annotations of individual spinal nerve roots, along with the reconstructed 3D lumbosacral spine model. We expect our dataset can provide a valuable platform to promote a wide range of spinal cord neuromodulation research and collaboration among neurorehabilitation engineers.

Methods

Participants. The MRI data was collected from 14 healthy adult volunteers (2 females and 12 males; Age: 23.21 ± 0.89 years; Height: 175.43 ± 8.22 cm; Weight: 71.14 ± 11.72 kg) between June 2023 and December 2023. Participants were publicly and randomly recruited from students in Fudan University. The inclusion criteria required participants to have no reported history of spinal cord injury (SCI), chronic back pain or stroke. Additional exclusion criteria were applied based on general guidelines for MRI safety and tolerance. All participants provided written informed consent, including an agreement for their data to be shared openly in an anonymous form. The experiment was approved by the ethics committee of Fudan University (approval number: FE23166I).

Image acquisition. The MRI scans were conducted at the Zhangjiang International Brain Imaging Center of Fudan University, using a 3T whole-body MRI system (MAGNETOM Prisma, Siemens Healthineers, Erlangen, Germany) equipped with a 20-channel head coil, an 18-channel body coil, and a spine coil. To locate different spinal structures, three MRI sequences were employed. (i) First, T2-weighted TSE (T2-TSE) was employed, with the following parameters: field of view = 240 mm × 240 mm, voxel size = 0.63 × 0.63 × 3.00 mm^3, TR/TE = 3500/104 ms, flip angle = 160°, readout bandwidth = 260 Hz per pixel, and the scan time = 3 minutes 22 seconds. To obtain images of the whole spine, T2-TSE sequences were applied 4 times targeting different segments. (ii) Second, double echo steady state sequence (DESS) was employed, with the following parameters were: field of view = 243 mm × 243 mm, voxel size = 1.27 mm isotropic, TR/TE = 10.95/3.86 ms, flip angle = 25°, readout bandwidth = 325 Hz per pixel, and the scan time = 2 minutes 23 seconds. (iii) Third, 3D high-resolution constructive interference in steady state (CISS) was employed with the following parameters: field of view = 288 mm × 288 mm, voxel size = 0.35 × 0.35 × 1.80 mm^3 or 0.30 × 0.30 × 2.00 mm^3 depending on the length of the participant's intumescentia lumbalis, TR/TE = 9.80/4.46 ms, flip angle = 50°, readout bandwidth = 305 Hz per pixel, turbo factor = 19 and the scan time = 29 minutes 30 seconds. The entire imaging protocol lasted approximately 1 hour including the time for preparation and localization.

Image preprocessing. The acquired MRI scans were converted from DICOM to Neuroinformatics Informatics Technology Initiative (NIfTI) format using dcm2niix (v1.0.20240202)[20] (https://www.nitrc.org/plugins/mwiki/index.php/dcm2nii:MainPage) and then organized following the Brain Imaging Data Structure (BIDS) format[21] using dcm2bids (v3.1.1)[22]. Example results are shown in Fig. 1.

Image postprocessing. Based on the MRI images acquired, the lumbosacral spine model for each subject was constructed. The pipeline is illustrated in Fig. 1. Annotation of the MRI images was performed using 3D Slicer (v5.4.0), involving two steps. Firstly, DESS and T2-TSE sequence images were annotated to locate ganglions at each target segment, aiding in determining the trajectory of nerve roots after exiting the intervertebral foramina. Secondly, annotations were carried out on the CISS sequence images to delineate the trajectories of individual nerve roots at each target segment, as well as to define the boundaries of the spinal cord white matter and cerebrospinal fluid and the position of the dura mater. In CISS images, nerve roots appear as black dots in a white background. Annotators traced the positions of nerve roots for each target segment on successive slices of CISS sequence images. The segment that each nerve root corresponds to was determined by its distance from the center of the spinal cord in each slice (i.e., closer proximity to the spinal cord center in a given slice indicates a lower spinal cord segment).

Two trained annotators participated in the annotation process, resolving uncertainties through consensus after discussions. The final annotation results were obtained by averaging the annotations of the two annotators. The annotation differences between the two annotators for different nerve roots are shown in Fig. 2. The figure indicates that the uncertainty in annotations gradually increases from L1 to S2. This trend is due to the increasing density of nerve roots within the field of view from L1 to S2. Although the annotation differences for the S1 and S2 nerve roots are relatively larger, they are still smaller compared to the width of the Medtronic 5-6-5 paddle lead (10 mm)[23] commonly used in EES, which is an important application relying on spine MRI. Therefore, the annotation differences between two annotators on S1 and S2 nerve roots can still be considered small enough and will not hinder related applications in practice. Furthermore, the placement of these implanted EES electrodes during implantation is primarily guided by the location of the L1 nerve root, the annotations of which between two annotators are highly consistent. In summary, the observed annotation discrepancies highlight the

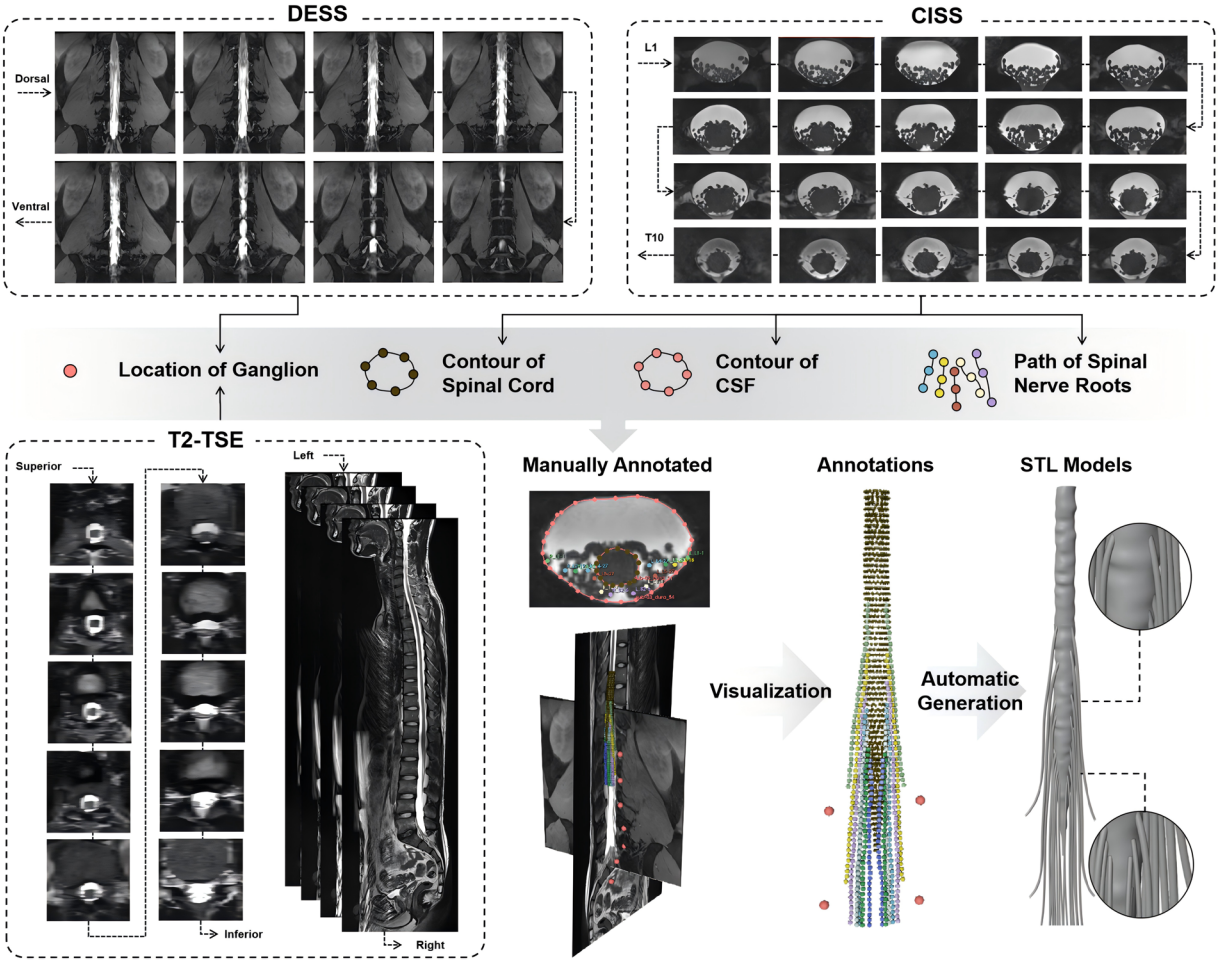

Fig. 1 Representative MRI data acquired from a healthy adult participant illustrating the human lumbosacral spine from multiple dimensions and the following postprocessing pipeline. T2-TSE sequence images delineate the spinal cord contour, while DESS sequence images highlight ganglion localization. Additionally, MRI images from the CISS sequence distinctly depict the distribution of spinal nerve roots in the lumbosacral spine. The geometry information was obtained through manual annotation and was subsequently utilized to automatically construct a comprehensive human lumbosacral model, encompassing structures such as the dura, cerebrospinal fluid, and the nerve roots spanning from L1 to S2.

inherent complexity of these physiological structures and can provide a valuable reference for evaluating the performance of machine learning algorithms developed using this dataset. The original data corresponding to Fig. 2 and the standard deviation of the annotation differences are provided along with the dataset.

Subsequently, based on these annotations, individual lumbosacral models (Fig. 3) for each subject were constructed using the open-source modeling software Blender (v4.0.2). Manual adjustment was applied to rectify the intersection issues caused by annotation bias. The Blender script used for modeling can be accessed via Github (https://github.com/Joshua-M-maker/SpineNerveModelGenerator).

Data Records

The dataset is available on Figshare[24]. All files were anonymized and organized according to the Brain Imaging Directory Structure (BIDS)[21] standard. The directory structure of the dataset is shown in Fig. 4. The MRI raw data and the corresponding .json files are contained in the branch */rawdata/sub-#/anat* of the root directory. Demographic information was included for each participant in the data file (*participants.tsv*) as per the BIDS standard. Within the */derivatives* branch, processed data are meticulously organized. Annotated points indicating key anatomical landmarks such as the dura mater, the boundary between the spinal cord white matter and cerebrospinal fluid, the ganglion, and the trajectories of nerve roots are cataloged under the */derivatives/markers* directory. Leveraging these annotations, detailed anatomical models are generated and stored in the */derivatives/model* subdirectory. Additionally, comprehensive image quality reports, generated using the MRIQC tool[19], are available within the */derivatives/anatqc* subdirectory.

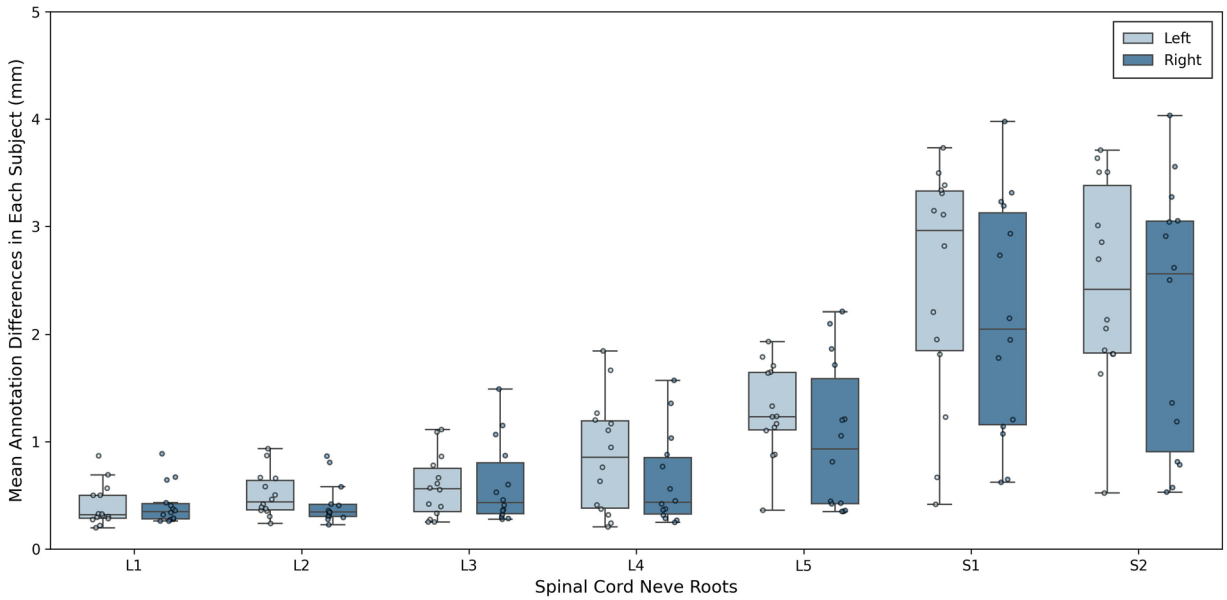

Fig. 2 Mean differences of annotations from two annotators for each subject, focusing on the L1 to S2 spinal cord nerve roots. Each data point represents the average annotation difference across different imaging slices. The differences were specifically measured by calculating the three-dimensional distances between the coordinates of corresponding points in the two sets of annotations.

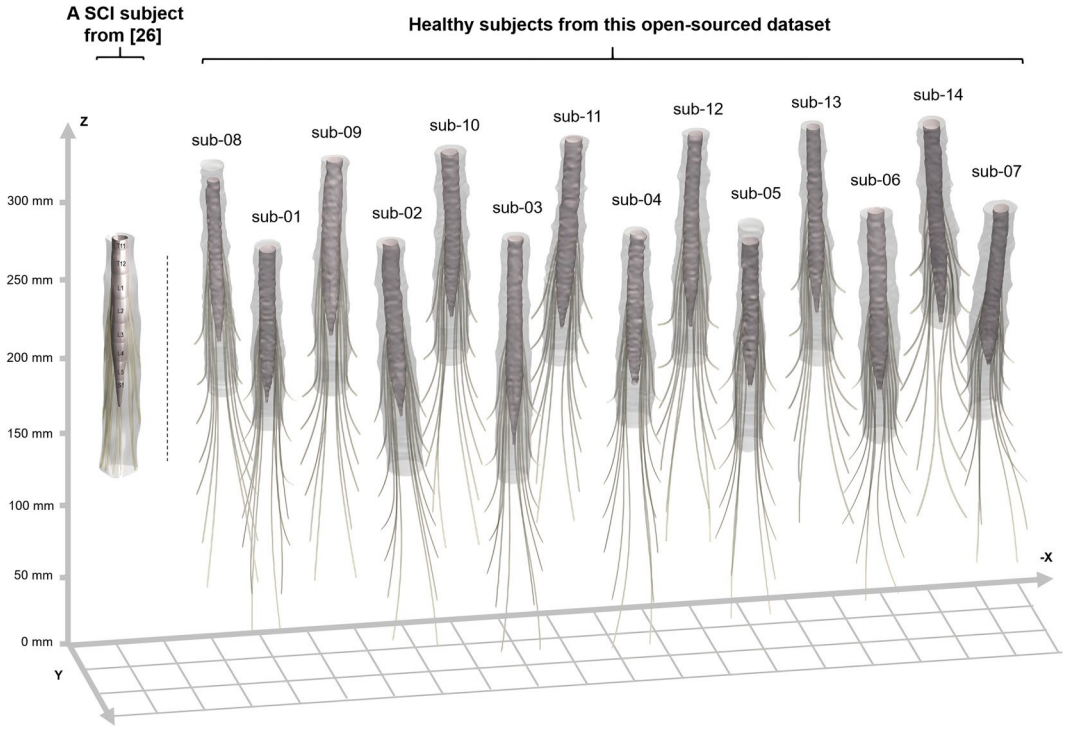

Fig. 3 Visualization of human lumbosacral models based on MRI data. The right 14 models were from 14 healthy adult participants in this work. Comparatively, the left model was from a spinal cord injury subject in another research[26] without open-sourced MR images, markers and models. Each model incorporates anatomical structures including the dura, cerebrospinal fluid, and nerve roots extending from L1 to S2. The direction of the coordinate axes is indicated. Spinal cord models were aligned by the highest planes of the dura structure to exhibit individual variability.

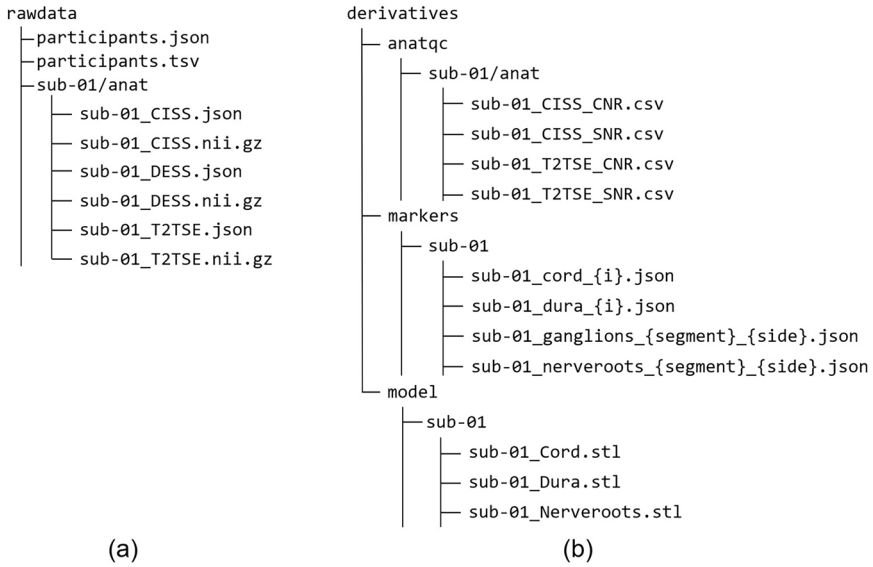

Fig. 4 Directory structure of the dataset. (**a**) Anonymized data with no additional processing are provided in the */rawdata/sub-#/anat* branch of the root directory, including CISS, DESS, and T2-TSE sequence imaging data. (**b**) Processed derivatives are organized in the */derivatives* branch according to their associated pipeline. Points marking the location of the dura mater (*/markers/sub-#/sub-#_dura_{i}.json*, where *i* refers to the number of CISS slices that demonstrate the dura), the boundary between the spinal cord white matter and cerebrospinal fluid (*/markers/sub-#/sub-#_cord_{i}.json*, *i* refers to the number of CISS slices that demonstrate the white matter), the ganglion (*/markers/sub-#/sub-#_ganglions_{segment}_{side}.json*, where *segment* is the targeted segment (L1 to S2), and *side* indicates left or right), and the trajectories of nerve roots (*/markers/sub-#/sub-#_nerveroots_{segment}_{side}.json*) are provided respectively. Based on the annotation, models (*/model*) are generated. Additionally, detailed image quality reports (*/anatqc*) for CISS, DESS, and T2-TSE raw data generated using MRIQC[19] are provided.

Technical Validation

To ensure the fidelity of image acquisition, we assessed image quality using two MRIQC image quality metrics (IQMs). Specifically, the signal-to-noise ratio (SNR) and contrast-to-noise ratio (CNR) were computed for each image slice. Since the DESS sequence was specifically designed for the target ganglion, the tolerance for image quality in the DESS sequence was relatively high. Consequently, quality evaluation was solely performed on image data from the T2-TSE and CISS sequences.

For the SNR estimation, we utilized MRIQC toolbox[19], where noise was defined as the weighted standard deviation of foreground, specifically the cerebrospinal fluid (CSF) and its internal spinal cord tissue. Additionally, CNR was computed to assess the contrast between the CSF and the spinal cord tissue, including the spinal cord nerve roots. The signal component was defined as the mean signal difference between these tissues, while the noise component was determined as the square root of the sum of the signal variances related to these tissues[25]. Segmentation of the cerebrospinal fluid and spinal cord nerve roots contours was performed by setting grayscale threshold via manual adjustments.

The resulting CNR and SNR values for the T2-TSE and CISS sequence images are shown in Fig. 5. The average CNR and SNR values of all participants in our dataset are consistently higher than 1.5. All images included in our dataset show good tissue contrasts and structural details.

Usage Notes

The dataset is available on Figshare[24]. We encourage researchers to use this dataset for their studies, with the stipulation of properly citing both the paper and the dataset. Our dataset offers comprehensive insights into the human lumbosacral anatomy, including trajectories of spinal cord roots and localization of ganglions, as depicted through T2-TSE, CISS, and DESS sequences. The derivative annotation-driven lumbosacral model serves as a fundamental resource for facilitating simulations for tailored EES therapy and further exploration into the variability of the human lumbosacral spine.

The detailed annotations of individual nerve roots in each MRI slice can also be used to develop machine learning and deep learning-based medical imaging models to automatically detect and trace the nerve roots in different MRI slices. The provided reconstructed 3D spine model based on manual annotations of nerve roots can be further used to develop an end-to-end deep learning model to directly reconstruct the 3D spine model from the MRI data.

Notably, the data in this dataset were collected from healthy subjects. As observed in Fig. 3, the overall morphology of the spinal cord in healthy subjects does not substantially differ from that of a patient (from a previous study[26]) with spinal cord injuries. Overall, we hope our dataset can be used to evaluate the performances

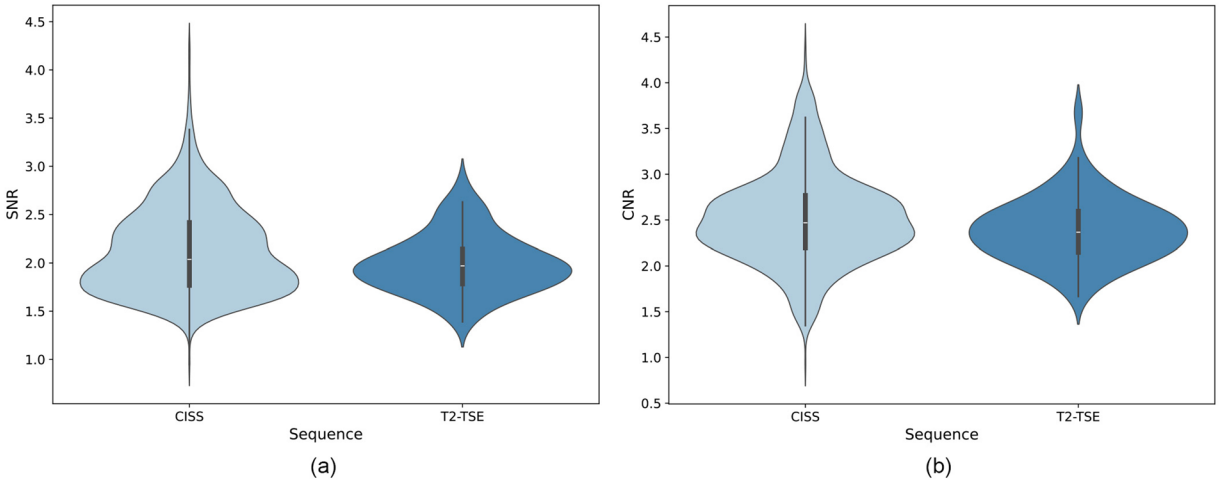

Fig. 5 Violin plots of image quality metrics (IQMs) for different acquisition protocols. (**a**) signal-to-noise ratio (SNR), and (**b**) contrast-to-noise ratio (CNR) for CISS and T2-TSE sequences.

of advanced algorithms on general healthy subjects. An algorithm generalized well across healthy subjects is expected to achieve satisfying performance on data from patients.

Code availability

The lumbosacral MRI data were processed employing several open-source software packages: dcm2niix (v1.0.20240202)[20], dcm2bids (v3.1.1)[22], and MRIQC (v23.1.0)[19]. Subsequent analysis was conducted utilizing Blender (v4.0.2) and Pyvista (v0.43.1). Modeling scripts are publicly accessible via GitHub (https://github.com/Joshua-M-maker/SpineNerveModelGenerator).

Received: 17 April 2024; Accepted: 23 September 2024;
Published online: 15 October 2024

References

1. Musienko, P., Heutschi, J., Friedli, L., Van Den Brand, R. & Courtine, G. Multi-system neurorehabilitative strategies to restore motor functions following severe spinal cord injury. *Experimental neurology* **235**, 100–109 (2012).
2. Won, S. M., Song, E., Reeder, J. T. & Rogers, J. A. Emerging modalities and implantable technologies for neuromodulation. *Cell* **181**, 115–135 (2020).
3. Bizzi, E., Tresch, M. C., Saltiel, P. & d'Avella, A. New perspectives on spinal motor systems. *Nature Reviews Neuroscience* **1**, 101–108 (2000).
4. Angeli, C. A., Edgerton, V. R., Gerasimenko, Y. P. & Harkema, S. J. Altering spinal cord excitability enables voluntary movements after chronic complete paralysis in humans. *Brain* **137**, 1394–1409 (2014).
5. Harkema, S. *et al.* Effect of epidural stimulation of the lumbosacral spinal cord on voluntary movement, standing, and assisted stepping after motor complete paraplegia: a case study. *The Lancet* **377**, 1938–1947 (2011).
6. Rowald, A. *et al.* Activity-dependent spinal cord neuromodulation rapidly restores trunk and leg motor functions after complete paralysis. *Nature medicine* **28**, 260–271 (2022).
7. Wenger, N. *et al.* Spatiotemporal neuromodulation therapies engaging muscle synergies improve motor control after spinal cord injury. *Nature medicine* **22**, 138–145 (2016).
8. Wagner, F. B. *et al.* Targeted neurotechnology restores walking in humans with spinal cord injury. *Nature* **563**, 65–71 (2018).
9. Angeli, C. A. *et al.* Recovery of over-ground walking after chronic motor complete spinal cord injury. *New England Journal of Medicine* **379**, 1244–1250 (2018).
10. Lorach, H. *et al.* Walking naturally after spinal cord injury using a brain–spine interface. Nature 1–8 (2023).
11. Canbay, S. *et al.* Anatomical relationship and positions of the lumbar and sacral segments of the spinal cord according to the vertebral bodies and the spinal roots. *Clinical anatomy* **27**, 227–233 (2014).
12. Pham, H. H., Trung, H. N. & Nguyen, H. Q. Vindr-spinexr: A large annotated medical image dataset for spinal lesions detection and classification from radiographs. PhysioNet (2021).
13. Liebl, H. *et al.* A computed tomography vertebral segmentation dataset with anatomical variations and multi-vendor scanner data. *Scientific data* **8**, 284 (2021).
14. Löffler, M. T. *et al.* A vertebral segmentation dataset with fracture grading. *Radiology: Artificial Intelligence* **2**, e190138 (2020).
15. van der Graaf, J. W. *et al.* Lumbar spine segmentation in mr images: a dataset and a public benchmark. *Scientific Data* **11**, 264 (2024).
16. Sudirman, S. *et al.* Lumbar spine mri dataset. Mendeley Data **2**, 2019 (2019).
17. Zhang, X. *et al.* Seuneter: Channel attentive u-net for instance segmentation of the cervical spine mri medical image. *Frontiers in Physiology* **13**, 2564 (2022).
18. Cohen-Adad, J. *et al.* Open-access quantitative mri data of the spinal cord and reproducibility across participants, sites and manufacturers. *Scientific data* **8**, 219 (2021).
19. Esteban, O. *et al.* Mriqc: Advancing the automatic prediction of image quality in mri from unseen sites. *PloS one* **12**, e0184661 (2017).
20. Li, X., Morgan, P. S., Ashburner, J., Smith, J. & Rorden, C. The first step for neuroimaging data analysis: Dicom to nifti conversion. *Journal of neuroscience methods* **264**, 47–56 (2016).
21. Gorgolewski, K. J. *et al.* The brain imaging data structure, a format for organizing and describing outputs of neuroimaging experiments. *Scientific Data* **3**, 160044 (2016).
22. Boré, A., Guay, S., Bedetti, C., Meisler, S. & GuenTher, N. Dcm2Bids, https://doi.org/10.5281/zenodo.8436509 (2023).

23. Rigoard, P. *et al*. Multicolumn spinal cord stimulation lead implantation using an optic transligamentar minimally invasive technique. *Neurosurgery* **73**, 550–553 (2013).
24. Liu, J. *et al*. An open-access lumbosacral spine mri dataset with enhanced spinal nerve root structure resolution. *figshare* https://doi.org/10.6084/m9.figshare.c.7372564 (2024).
25. Magnotta, V. A., Friedman, L. & BIRN, F. Measurement of signal-to-noise and contrast-to-noise in the fbirn multicenter imaging study. *Journal of digital imaging* **19**, 140–147 (2006).
26. Mesbah, S. *et al*. Neuroanatomical mapping of the lumbosacral spinal cord in individuals with chronic spinal cord injury. *Brain Communications* **5**, fcac330 (2023).

Acknowledgements

This work is Supported by Shanghai Municipal Science and Technology Major Project (No. 2018SHZDZX01), ZJ Lab, Shanghai Center for Brain Science and Brain-Inspired Technology, and 111 Project (No. B18015). MRI equipment and acquisition support were provided by Zhangjiang International Brain Imaging Center, Fudan. The authors thank all volunteers for participating in the acquisition.

Author contributions

Participant recruitment and Data acquisition: Jionghui Liu; Annotation: Jionghui Liu and Linhao Xu; Figures design and illustration: Jionghui Liu and Wenqi Zhang; Data processing, model generation and writing the article: Wenqi Zhang; Initial conception and overall design: Yuxing Zhou and Fumin Jia; Quality control: Linhao Xu; MRI sequence adjustment: Ying-Hua Chu. All authors provided feedback and approved the final manuscript.

Competing interests

The authors declare no competing interests.

Additional information

Correspondence and requests for materials should be addressed to F.J.

Reprints and permissions information is available at www.nature.com/reprints.

Publisher's note Springer Nature remains neutral with regard to jurisdictional claims in published maps and institutional affiliations.